Highly sensitive detection of DNA damage of live cells by SERS and electrochemical measurements using flexible gold nanoelectrode

Jing Zhou[a], Dan Yang[a], GuohuiLiu[a], Siying Li[a], WennanFeng[a], Guocheng Yang[a], Jin He[b*] and Yuping Shan[a*]

[a]School of Chemistry and Life Science, Advanced Institute of Materials Science, Changchun University of Technology, Changchun 130012, China. E-mail: shanyp@ciac.ac.cn.

[b]Physics Department, Florida International University, Miami 33199, United States. E-mail: jinhe@fiu.edu.

Table of contents

S1. The fabrication and characterization of fGNEs

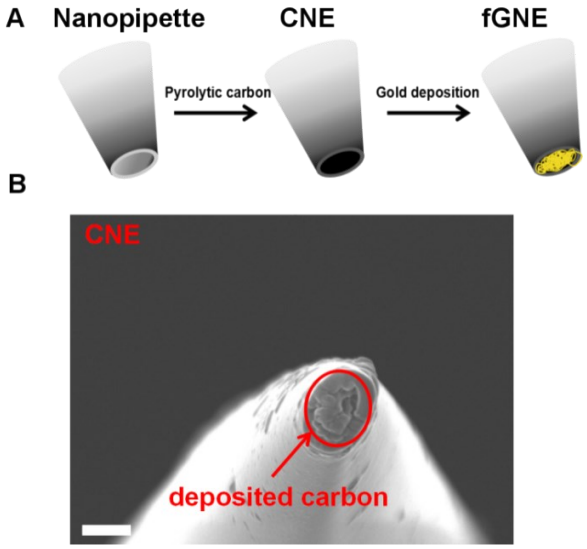

Fig. S1 The fabrication of fGNE. (A) The schematic diagram for the fabrication of a fGNE via nanopipette and CNE. (B) SEM image of carbon nanoelectrode (CNE), which is inside red circle. The scale bar is 100 nm.

The procedure of fabricating flexible gold nanoelectrode (fGNE) is shown in Fig. S1A. Initially, the clean capillaries were pulled using a P-2000 puller to form nanopipettes. The ionic I-V curves of nanopipettes were measured by using a source-measure unit (Keithley 2636A). The bias was applied between two Ag/AgCl wire electrodes, one was inserted in the nanopipette barrel and the other was placed in the bath solution. As described in detail before,[1] the diameter of the nanopore of the prepared nanopipette was estimated via measuring the nanopore conductance (*Gp*) by the following formula:

$$D = \frac{Gp}{K}\left(\frac{1}{\pi \tan\theta}\right) \qquad (1)$$

Where *Gp* is the conductivity of nanopores, which is determined by I-V measurements in 10 mM PBS. The I-V curves of 20 nanopipettes are shown in Fig. S2A, and the *Gp* is determined from the linear section of the I-Vs at low bias. The obtained *Gp* is 0.96 ± 0.03 S (Fig. S2B). The half-cone angle of the nanopipette was

measured as θ=6.2 ± 0.5°. The derived nanopore diameter mean value is about 102 ± 16 nm (Fig. S2C).

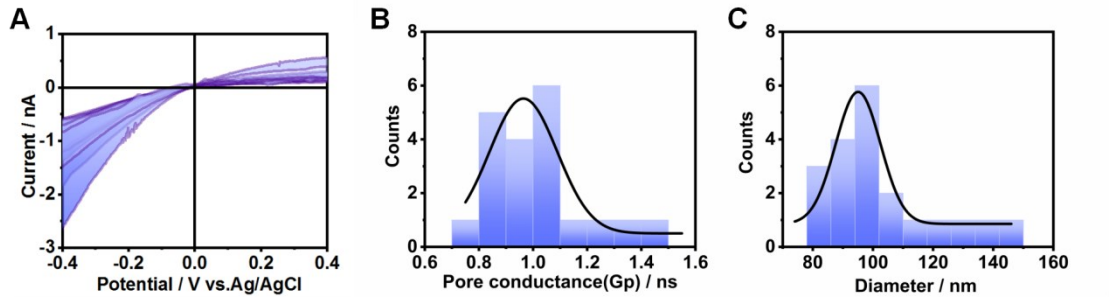

Fig. S2 Electrical characterization of the nanopipettes. (A) The I-V curves of the nanopipettes in 10 mM PBS. (B) The histograms of Gp for the nanopipettes (N=20). (C) The distribution of the derived nanopore diameter. The solid line is Gaussian fit to the histogram (N=20).

The carbon nanoelectrode (CNE) was formed through butane pyrolysis in the nanopipette with a humidity of about 45%.[2] After forming CNE, a copper wire (0.1 mm diameter) was connected to the backend of the CNE using silver conductive glue. The SEM image of a prepared CNE tip is shown in Fig. S1B. The gold was deposited on the exposed CNE surface by electro-deposition method.[3]

The effective surface area of CNEs and fGNEs was characterized by cyclic voltammograms (CVs) using a potentiostat (CHI 852D). An Ag/AgCl wire electrode was used as the quasi-reference electrode and a Pt wire was used as the counter electrode. The 1 mM $Ru(NH_3)_6Cl_3$ was added to the bath solution (10 mM PBS) as redox mediator.

The effective area A_{eff} of the electrode can be calculated based on the diffusion limited current I_{diff} by equation (2) below:

$$I_{diff}=4nFDCA_{eff} \quad (2)$$

where n is the number of transferred electron, F is the Faraday constant, D is the diffusion coefficient of ruthenium hexamine, and C is the concentration. Based on the measured I_{diff}, the A_{eff} of the fGNEs is significantly larger than that of the CNEs (Fig. S3). However, from the SEM images, the size increase of the protruded center

electrode from CNE to fGNE is not significant after gold deposition. Therefore, we speculated that the gold should also deposite on the glass surface near the CNE.

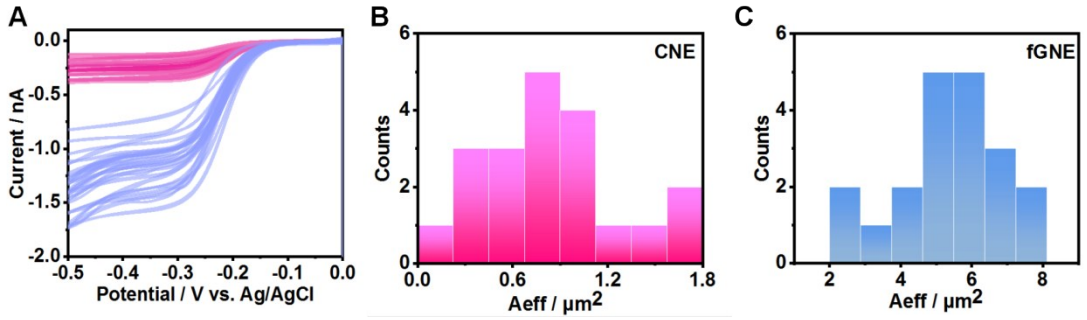

Fig. S3 Electrochemical characterization of CNE and fGNE. (A) The CVs of CNEs (pink) and fGNEs (blue) in 10 mM PBS containing 1 mM $Ru(NH_3)_6Cl_3$. All CVs were performed at a scan rate of 50 mV/s. The histograms of effective area for CNEs (B) and fGNEs (C). (N=20)

To further confirm the successful deposition of gold, freshly prepared fGNE was examed by CV in 0.5 M H_2SO_4. The oxidation and reduction peaks of gold can be observed in Fig. S4. Both peaks are also quite stable in 25 repeated cycles.

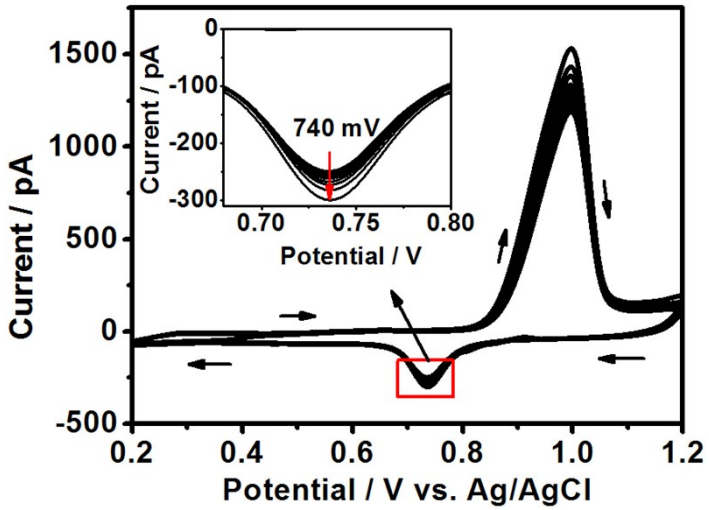

Fig. S4 The 25 continuous CVs of a freshly prepared fGNE in 0.5 M H_2SO_4. The scan rate is 50 mV/s. The inset shows the reduction peak of gold near potential +740 mV.

S2. UV-Vis extinction spectroscopy of AuNPs and AuNPs-8-OHdG

We followed the previously reported method of chemical reduction with sodium

citrate to prepare AuNPs about 45 nm size.[4] The AuNPs were then modified by 8-OHdG in DI water at a molar ratio of 1:5. Then the mixed solution was stirred at room temperature for 30 min. The conjugates were purified by centrifugal filtration method using aultra filter (PALL Life Sciences) with a 3kD Molecular Weight Cutoff (MWCO) value to remove free 8-OHdG molecules in solution. The 8-OHdG modified AuNPs were examed by UV-vis extinction spectroscopy. After surface modification, the NP's localized surface plasmon resonance (LSPR) peak near 520 nm decreased and slightly shifted. In contrast, the adsorption increased greatly below 300 nm, which is due to the presence of 8-OHdG on the AuNP surface. These changes indicate that 8-OHdG molecules can interact strongly with gold and attach to the surface of AuNPs.[5]

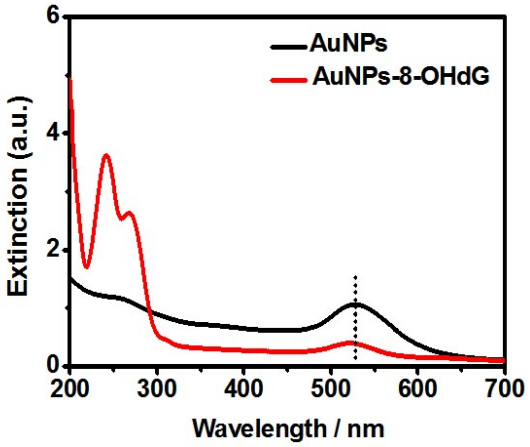

Fig. S5 UV-Vis spectra of AuNPs (~45 nm) (black) and AuNPs-8-OHdG (red).

S3. Preparation and characterization of AgNPs

The AgNPs are prepared by chemical reduction with sodium citrate.[6] 8.49 mg $AgNO_3$ was dissolved in 50 ml of DI water. The solution was heated and stirred to boil. Then 1 ml sodium citrate solution was added to the above solution and the solution was heated for 30 min. Subsequently, the solution was cooled to room temperature. In the whole process, the solution was stirred continuously. The prepared AgNPs were sonicated and drop-casted on a silicon wafer for SEM imaging (Fig. S6A). The size of AgNPs was analyzed based on the SEM images. By fitting

Gaussian function to the size distribution histogram, the mean AgNP diameter is 59 ± 24 nm (Fig. S6B).

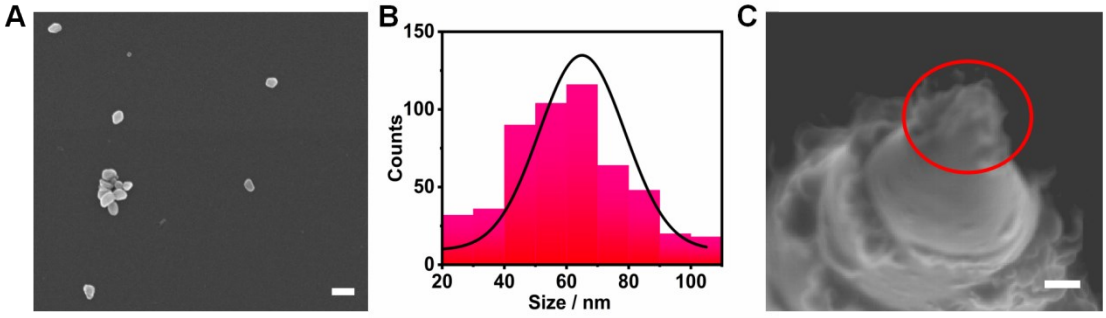

Fig. S6 SEM characterization of AgNPs. (A) SEM image of AgNPs. The scale bar is 100 nm. (B) The size distribution of AgNPs (N=528) with the Gaussian fit (black curve). (C) SEM image of a AgNPs covered fGNE apex (inside the red circle), which is tethered with 8-OHdG molecules. The scale bar is 100 nm.

S4. DPVs of G and 8-OHdG using CNEs

We also used DPV to measure the mixtures. As shown in Fig. S7A, the oxidation peaks of 8-OHdG (0.41V) and G (0.71 V) can be identified in the mixture of 10 μM G and 8-OHdG. In Fig. S8B, the oxidation peak of 8-OHdG near 0.42 V can be observed with the presence of four bases (A, T, C, G). The oxidation peaks of G (0.82 V) and T (1.20 V) can also be clearly identified. The results in Fig. S7 were conducted in DI water. Similar results were observed when the DPV were conducted in cell culture medium MEM though all the oxidation peaks were slightly right-shifted.

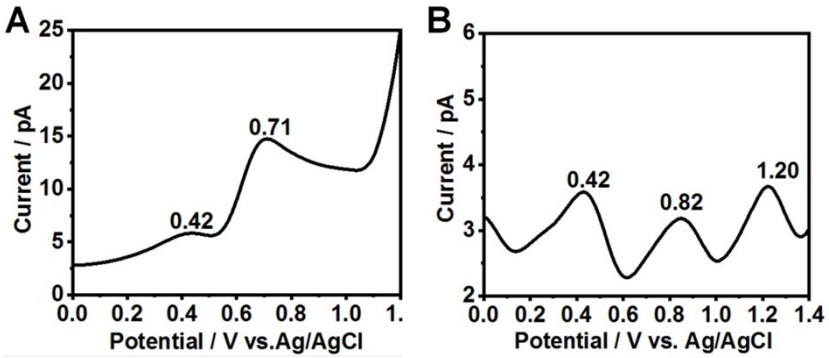

Fig. S7 The DPV of mixtures. (A)The DPV for the mixture of G (10 μM) and 8-OHdG (10 μM). (B) The DPV forthe mixture of 10 μM A, T, G, C and 8-OHdG. The

scan rate is 50 mV/s.

Fig. S8A and C show the DPVs of G and 8-OHdG at different concentrations, which are adsorbed to CNEs. The DPV peak is lower than that of fGNEs at the same molecule concentration. As shown in Fig. S8B and D, the linear range of CNEs is divided into two sections: 0-100 nM and 100-500 nM. The slopes for G are 0.0017 and 0.0043 pA nM^{-1}, while the slopes for 8-OHdG are 0.0026 and 0.0061pA nM^{-1}, respectively.

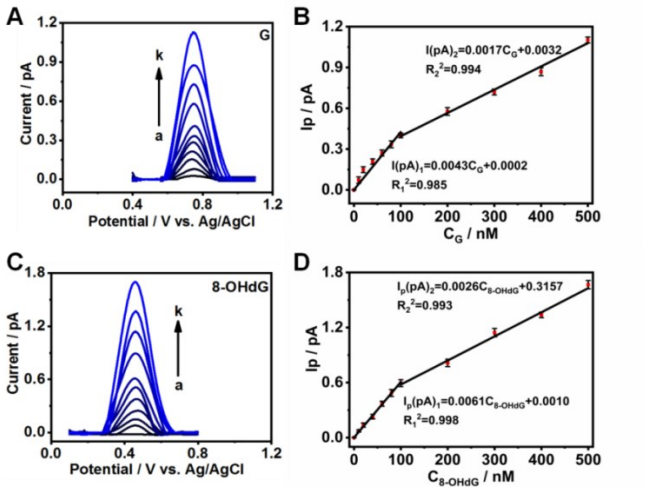

Fig. S8 Electrochemical measurements of G and 8-OHdG with CNEs. (A, C) DPVs for G and 8-OHdG at different concentrations (from a to k, 0 nM, 10 nM, 20 nM, 40 nM, 60 nM, 80 nM, 100 nM, 200 nM, 300 nM, 400 nM and 500 nM, respectively) in 10 mM PBS. The scan rate is 50 mV/s. (B, D) The peaks current (ΔI_P) at different concentrations of G and 8-OHdG. The error bars represent the standard deviations of three experiments.

S5. Detecting the four-electron oxidation products of G with DPV and SERS measurements

When the scanning speed is 50 mV/s, G undergoes the four-electron oxidation to

become oxidized 8-oxoguanine (8-OXOG (OX)). After the conversion, the oxidation peak in the DPV is up-shifted from +0.71V to +0.78 V. The oxidation products were also measured by SERS. As shown in Fig. S9C, the peaks at 609 cm^{-1}, 1063 cm^{-1}, and 1443 cm^{-1} are consistent with the DFT calculated peaks (Table S2), which proves that the four-electron transfer of G is established. More peaks appear in the SERS spectrum of 8-OXOG (OX) than in the spectrum of 8-OXOG.

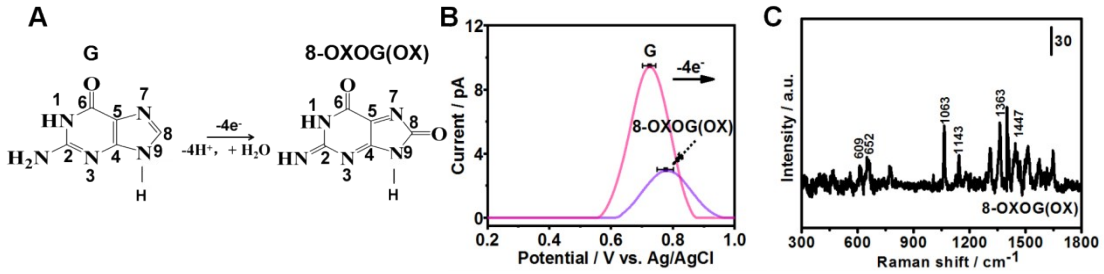

Fig. S9 Electrochemistry and SERS detection of G before and after electron transfer. (A) Electrochemical oxidation mechanism diagram of G on the surface of fGNEs with the scan rate of 50 mV/s. (B) The DPVs of G and 8-OXOG (OX) (after four-electron transfer). The error bars represent the standard deviation. (C) SERS spectrum of adsorbed 8-OXOG (OX) on the apex of fGNE. The 8-OXOG (OX) molecules are formed after four-electron oxidation of G.

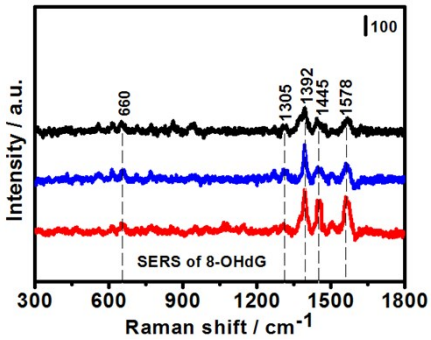

Fig. S10 SERS spectra of 8-OHdG on three different fGNEs, where were immersed in DI water with 0.1 nM 8-OHdG.

S6. SERS of four DNA bases adsorbed on fGNEs

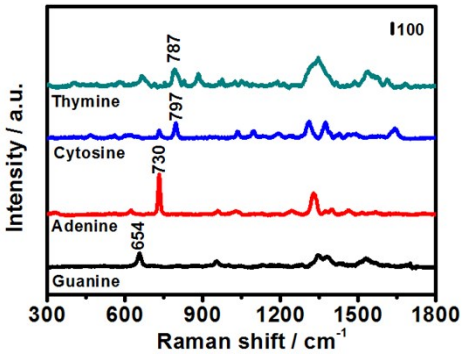

Fig. S11 SERS spectra of four DNA bases (G, A, C, and T) attached to fGNEs in 10 μM DNA base solution. The characteristic peaks of G, A, C and T are at 654, 730, 797, and 787 cm^{-1}, respectively.

S7. SERS spectra of 8-OHdG on fGNE after collecting 8-OHdG with various concentrations in MEM solution

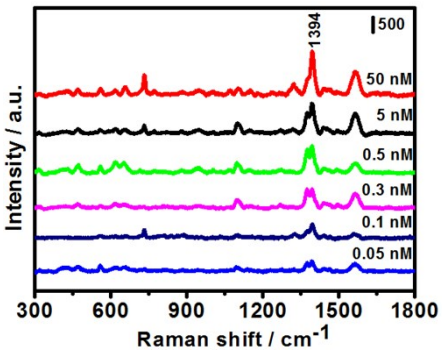

Fig. S12 The SERS spectra of fGNEs after collecting 8-OHdG with various concentrations in MEM solutions for 40 min.

S8. Trypan blue cell viability test

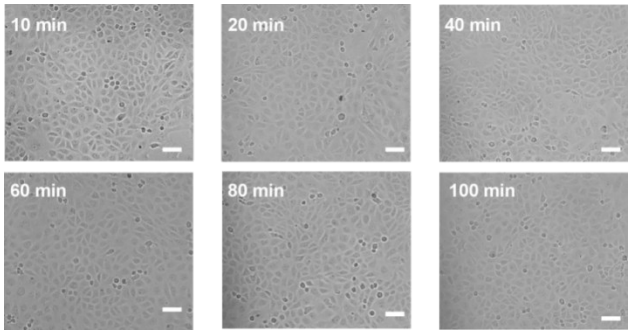

Fig. S13 Optical images of Vero cells. The cells were first treated with 20 μM K_2CrO_4 (final concentration) for 2 h and then cultured in fresh serum-free medium for different time. For each time point, 0.4% trypan blue was added to MEM in a 1:1 (v:v) ratio 10 min early. The dead cells appear as dark gray color in the black-white images. The scale bar is 100 μm.

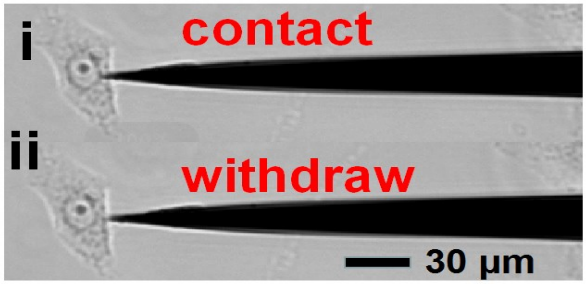

Fig. S14 The optical microscope images of a fGNE tip approach and slightly touch the Vero cell membrane (i) and then withdraw a few microns from the cell (ii). The fGNE was controlled by a micromanipulator. The scale bar is 30 μm.

S9. SERS spectra of 8-OHdG on fGNEs after collecting 8-OHdG for different time in untreated cells

To assess the 8-OHdG collection capacity of fGNE, 0.1 nM 8-OHdG was added to the MEM medium with untreated live Vero cells. By applying a constant bias of -70 mV to the fGNE, we keep the fGNE in the medium for different time. The SERS

spectra were measured from the fGNE after different collection times. As shown in Fig. S15, the characteristic vibration peak intensity I_{1394} in the SERS spectra gradually increases with the increase of collection time. The increase trend remains up to 100 min.

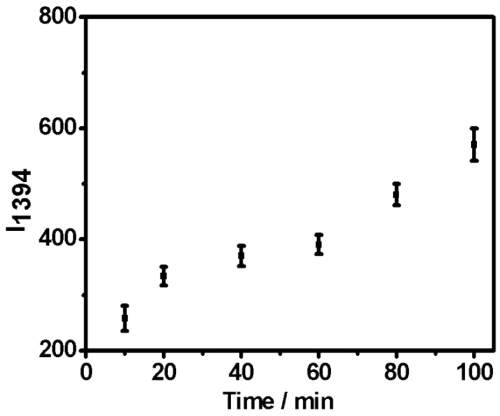

Fig. S15 The I_{1394} change as a function of collection time. 0.1 nM 8-OHdG was added to the MEM media with untreated Vero live cells. The error bar represents standard deviations.

Table S1. Characteristic normal Raman and SERS peaks of G resulted from theoretical calculation and experimental results.[7, 8]

Calculated / cm^{-1}	**Powder / cm^{-1}**	**SERS of fGNE / cm^{-1}**	**Assignments**
663	643	660	whole-molecule ring breathing
916	934	916	def R5, qz N7-C8-N9
1316	1342	1321	bend N1-H, N10-H12, str C2-N10
1390	1381	1380	str N1-C2, C4-C5, bend N9-H,
1533	1529	1527	str N3-C4, C4-N9, bend N9-H

R5, five-membered ring; R6, six-membered ring; bend, bending; def, deformation;

rock, rocking; sciss, scissoring; sqz, squeezing; str, stretching; wag, wagging.

Table S2. Raman characteristic peaks of 8-OXOG (OX) resulted from theoretical calculation and experimental results.[9]

Calculated / cm^{-1}	**SERS of fGNE/ cm^{-1}**	**Assignments**
604	609	whole-molecule ring breathing
658	652	str N1-H, N2-C4
1081	1063	def R5, R6, rock N9-H
1158	1143	wag N7-H, rock NH2
1368	1363	str C4-C5, C4-N9
1439	1443	str N7-C8, , bend N7-H, C8-H

References

1. N. Panday, G. Qian, X. Wang, S. Chang, P. Pandey and J. He, *ACS Nano*, 2016, **10**, 11237-11248.
2. J. Clausmeyer, P. Wilde, T. Lffler, E. Ventosa and W. Schuhmann, *Electrochemistry Communications*, 2016, **73**.
3. D. Yang, G. Liu, H. Li, A. Liu, J. Guo, Y. Shan, Z. Wang and J. He, *The Analyst*, 2020, **145**, 1047-1055.
4. Z. Li-Bo, L. Dan, Y. Hua-Lun, D. Zhen-Juan, Z. Qiu-Yuan, L. I. Yi and W. Hong-Bin, *Journal of Yunnan Minzu University(Natural ences Edition)*, 2017.
5. K. Shrivas, N. Nirmalkar, S. S. Thakur, R. Kurrey, D. Sinha and R. Shankar, *RSC Advances*, 2018, **8**, 24328-24337.
6. ShekharAgnihotri, SoumyoMukherji and SuparnaMukherji, *Rsc Advances*, **4**.
7. R. P. Lopes, M. P. M. Marques, R. Valero, J. Tomkinson and L. A. E. B. de Carvalho, *Spectroscopy: An International Journal*, 2012, **27**, 273-292.
8. B. Giese and D. McNaughton, *Physical Chemistry Chemical Physics*, 2002, **4**, 5161-5170.
9. B. Pergolese, A. Bonifacio and A. Bigotto, *Physical Chemistry Chemical Physics*, 2005, **7**, 3610.